第50卷第10期 中国科学技术大学学报 Vol. 50, No. 10
2020年10月 JOURNAL OF UNIVERSITY OF SCIENCE AND TECHNOLOGY OF CHINA Oct. 2020
Received: 2020-09-02; Revised: 2020-10-20 doi:10.3969/j.issn.0253-2778.2020.10.001

Compressibility effect on shock-induced air/helium chevron interface evolution

GUO Xu, ZHAI Zhigang, LUO Xisheng
Department of Modern Mechanics, University of Science and Technology of China, Hefei 230027, China

Abstract: Shock tube experiments of a periodic air-helium chevron interface impacted by a planar shock wave are conducted. Effects of the compressibility and the initial amplitude on the perturbation growth are highlighted. For small initial amplitudes, the shock Mach number has limited effects on the reliability of the linear model. For high initial amplitudes, however, the linear model is generally invalid because the high amplitude effect will reduce the linear growth rate. Under the high initial amplitude condition, the increase of the shock Mach number further aggravates the discrepancy of the experimental result with the theoretical prediction. By considering the high amplitude effect and the high Mach number effect, the linear growth rate of the interface with high initial amplitude impacted by a strong shock wave can be well predicted. The compressibility effect induced by the incident shock wave can be illustrated by the material compression and the geometric compression of the interface, and the latter is found to be dominant. In the nonlinear regime, some nonlinear models proposed for single-mode interfaces are verified to be valid only at very early stages.

Key words: Richtmyer-Meshkov instability; multi-mode
CLC number: V211.7 **Document code**: A

0 Introduction

The intersection of a shock wave with a misaligned density gradient created by a fluid interface will result in the creation of the Richtmyer-Meshkov instability (RMI). This instability was examined by Richtmyer[1] in his theoretical work, and later by Meshkov[2] in his experiments. The RMI occurs in a variety of applications. In astrophysics, it has been used to explain the lack of stratification in supernova products and is required in stellar evolution models[3,4]. In combustion systems with shock-flame interactions, it plays an important role in deflagration-to-detonation transition[5], and it can be used to promote mixing in supersonic air-breathing engines[6,7]. The application that has motivated the majority of studies is inertial confinement fusion (ICF), a technology with the potential to demonstrate highly efficient carbon-free energy production. In ICF, the RMI occurs at the interfaces of the deuterium fuel target during its laser driven compression causing mixing of the high density, high temperature core with surrounding material and greatly reducing the fusion yield[8,9]. Due to its importance to a variety of applications, the RMI has received much attention and a series of comprehensive reviews[10-15] have been published in the past decades.

Experiments on the RMI under laboratory conditions are usually carried out in shock tubes. The shock wave is created by the sudden release of a high pressure volume into a low pressure volume initially separated by a plastic or metal diaphragm. The density gradient is created by the interface of two fluids of different densities, and is usually perturbed to misalign the pressure gradient induced by the shock wave. A variety of methods for perturbing the fluid interface have been developed, such as the membrane technique[16-19] or membraneless technique[20-22]. When the incident shock wave refracts from the light (heavy) fluid to the heavy (light) fluid, the interface between two fluids is generally called the light-heavy (heavy-light) one. Richtmyer[1] first theoretically studied the RMI in terms of a light-heavy single-mode interface with a small initial amplitude and proposed the impulsive model to describe the linear growth behavior of the perturbation. Since then, extensive studies on the perturbation growth of the light-heavy single-mode interface have been performed[2,20,23-27], and the impulsive model has been validated qualitatively and quantitatively. In practical

Citation: GUO Xu, ZHAI Zhigang, LUO Xisheng. Compressibility effect on shock-induced air/helium chevron interface evolution. J. Univ. Sci. Tech. China, 2020, 50(10): 1279-1290.

applications, actually, the random perturbations with infinite many modes generally exist on the interface, and the coupling between different modes complicates the flow. Recently, a series of experiments on developments of light-heavy chevron interfaces[28-31] and light-heavy inclined interfaces[22,32-35] accelerated by shock waves have been carried out. A chevron interface was generated by the soap film technique and the early-time evolution of the RMI has been highlighted[28-31,36]. Specifically, the mode coupling[31] and the bubble competition[36] have been investigated. An inclined interface (half the chevron interface) was generated by the gas diffusion technique, and the late-time evolution of the RMI especially the turbulent flow characteristics have been emphasized[22,32-35].

Relative to the light-heavy interface, the heavy-light interface receives less attention. In ICF, note that the central capsule is made of thin concentric spherical shells, generally containing the outer shell of the ablator, the middle shell of the solid DT fusion fuel and the inner shell of the DT vapor[9]. Due to the difference in density, the outer and the middle shells constitute a light-heavy interface, whereas the middle and the inner shells constitute a heavy-light interface. As a result, the heavy-light interface is closer to the center of the capsule, and the induced hydrodynamic instability of the heavy-light interface is crucial to the ignition. Meyer & Blewett[37] investigated the development of a heavy-light single-mode interface impacted by a planar shock wave and found that the impulsive model was not applicable to predicting the heavy-light interface evolution unless the amplitude term of the impulsive model was adjusted, and a linear model (the MB model) applicable to the heavy-light case was proposed. In the experiments performed by Jourdan & Houas[38], the heavy-light interface only consists of bubbles, but the spikes are replaced by flat parts. Their results indicated that the linear growth rate of such a heavy-light interface perturbation can be predicted by the impulsive model[1], which is inconsistent with the conclusion reached by Meyer & Blewett[37]. Note that the interface adopted in the experiments is not a pure single-mode one, because the flat parts exist and could affect the bubble evolution[30]. Besides, the initial interface is uncontrollable, and there are many short-wavelength disturbances on the interface, which also affect the amplitude growth. Mariani et al[39] used the stereolithography to design the membrane supports such that the initial interface is more controllable than previous work[38]. The developments of the air-helium interface were well predicted by the model. Recently, Ma et al[40] experimentally and numerically investigated the RMI of a heavy-light single-mode interface, and found that the MB model gives a good prediction to the linear growth rates.

The shock Mach number in shock-tube experiments mentioned above is low, and thus the compressibility effect is insignificant. As Mikaelian[41] stated, the compressibility effect can inhibit the perturbation growth rate. For a light-heavy interface, Aleshin et al[42] studied the development of an Ar-Xe interface accelerated by a planar shock wave with a Mach number of 2.5. The results showed that the impulsive model can approximately predict the linear growth rate if initial amplitudes are small, but overestimate the linear growth rate if initial amplitudes are high. For a heavy-light interface, the evolution of a Be-foam interface impacted by a strong shock with a Mach number of 15.3 in laser driven experiments has been investigated. Similarly, the MB model can predict the growth rate of the perturbation when the initial amplitude is small even though the shock Mach number is extremely high. As a result, the high amplitude effect rather than the high Mach number effect is the dominant one, as proved by Rikanati et al[43] and Sadot et al[44] in their shock-tube experiments.

To highlight the compressibility effect on the perturbation growth, evolution of the air-SF_6 chevron interface accelerated by a planar shock wave with different Mach numbers has been investigated in our previous work[45]. The results indicated that except for the transverse waves effect, the shock proximity effect[43-46] where the proximity of the transmitted shock wave to the interface also inhibits the perturbation growth. However, Glendinning et al[46] pointed out that for a heavy-light configuration where the transmitted shock waves move much faster than the shocked interface, the shock proximity effect can be insignificant even for very high Mach numbers, unless a high initial amplitude is imposed on the interface. Therefore, for two different interface configurations (light-heavy or heavy-light), the compressibility effect is different. To figure out the difference of the compressibility effect between them, evolution of the heavy-light chevron interface accelerated by a planar shock wave with different Mach numbers needs to be investigated, which

motivates the current work.

In our previous work[47], a chevron air-helium interface was generated by the soap film technique, and the effect of the initial amplitude on the amplitude growth has been highlighted. The results verified the reliability of the MB model for predicting the growth of the interface with small initial amplitude after the phase reversal. Note that in the previous work[47], only one shock Mach number is involved and the experimental duration was so short that the nonlinear behavior of the amplitude growth was absent. Furthermore, the chevron interface with flat portions at both sides is non-periodic, and the flat portions have non-negligible influences on the adjacent interface development[30]. In this work, a periodic chevron air-helium is generated by the soap film technique, and different shock Mach numbers are involved to highlight the compressibility effect induced by incident shock wave on the perturbation growth.

1 Experimental methods

The initial interface consists of three chevron interfaces in the middle and two flat interfaces at both sides, as shown in Fig. 1. The flat parts connecting the wall have been verified to have limited effects on the central interface development[30], and we measure the central interface to calculate the perturbation growth rate. Two initial vertex angles ($\theta = 160°$ and $120°$, corresponding to two amplitude-wavelength ratios ($a_0/\lambda = 0.044$ and 0.144 with a_0 and λ being the initial amplitude and wavelength, respectively), are involved. The initial interface is generated by the soap film technique which has already succeeded in creating interface with different shapes in the previous work[27,28,31,36]. Therefore, the interface formation process will be briefly described here. The interface framework is first manufactured by acrylic plates, and then thin wires (0.128 mm in diameter) are introduced at the corner to avoid pressure singularity. In this work, only one wire is needed at each corner because $\theta \geqslant 120°$[28,48]. The interface is generated by pulling a rectangular frame along the edges of the framework with the solution prepared (made of 60% clean water, 20% concentrated soap liquid and 20% glycerin by volume). The boundary layer effect and the three-dimensional effect on the interface evolution are verified to be limited[28,30].

After the interface formation, the interface framework is first inserted into the test section. Then helium is injected into the right side of the interface through a hole at the end of the test section, and air is discharged from the other hole. An oxygen concentration detector is placed near the hole to ensure the helium purity in the test section. Before the shock wave contacts the interface, the helium and air will diffuse through the soap film, causing the mixing of the gases. In this work, the gas concentrations at both sides of the interface are determined by the velocities of the incident and transmitted shock waves measured from the schlieren images and one-dimensional (1D) gas dynamics theory. The detailed experimental parameters are listed in Tab. 1.

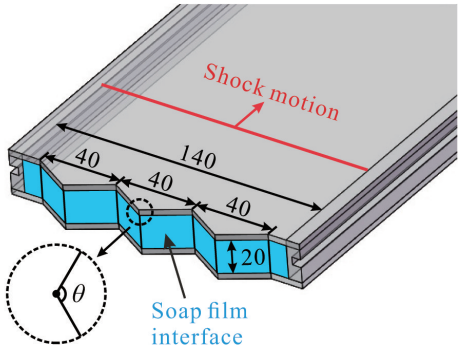

Fig. 1 The interface framework manufactured by acrylic plates. θ represents the initial vertex angle. The unit of numbers is mm

The experiments are carried out in the same shock tubes as that in the previous work[28,47]. Polyester diaphragms of different thicknesses are placed between the driver and driven sections to vary the incident shock Mach number (Ma). The incident shock Mach number in this work ranges from 1.2 to 1.9, as listed in Tab. 1. The flow field is illuminated by a Xenon light source (CEL-HXF300), and captured by a schlieren system combined with a high-speed video camera (FASTCAM SA5, Photron Limited). The frame rates of the camera are 50000 f. p. s for $\theta = 120°$, and 75000 f. p. s for $\theta = 160°$.

2 Results and discussion

The interface morphology and the amplitude growth in linear and nonlinear stages will be discussed in this section. The effects of the initial amplitude and the shock Mach number on the interface evolution will be investigated. The compressibility effect induced by the incident shock wave on the perturbation growth for light-heavy and heavy-light interfaces will be highlighted. Note that the initial time in this work is defined as the moment when the phase reversal is completed.

Tab. 1 Experimental parameters for eight cases. Ma, incident shock Mach number; V_l (V_r), volume fraction of helium at the left (right) side of the interface; A and A^+, pre- and post-shock Atwood number, respectively; U_c, jump velocity for a flat interface calculated by 1D gas dynamics theory; U_i and U_t, incident and transmitted shock wave velocities, respectively. The velocity unit is m/s.

θ	Ma	V_l/%	V_r/%	A	A^+	U_c	U_i	U_t
160	1.18	14.4	95.0	−0.657	−0.663	138	437	968
	1.40	2.8	96.3	−0.703	−0.713	277	490	1107
	1.73	3.0	98.0	−0.724	−0.736	468	606	1311
	1.84	2.0	98.0	−0.726	−0.737	526	642	1362
120	1.19	9.3	90.5	−0.613	−0.621	135	427	882
	1.37	9.2	93.0	−0.645	−0.656	258	496	1022
	1.66	8.9	94.2	−0.661	−0.674	423	597	1182
	1.78	10.8	92.3	−0.631	−0.645	487	649	1202

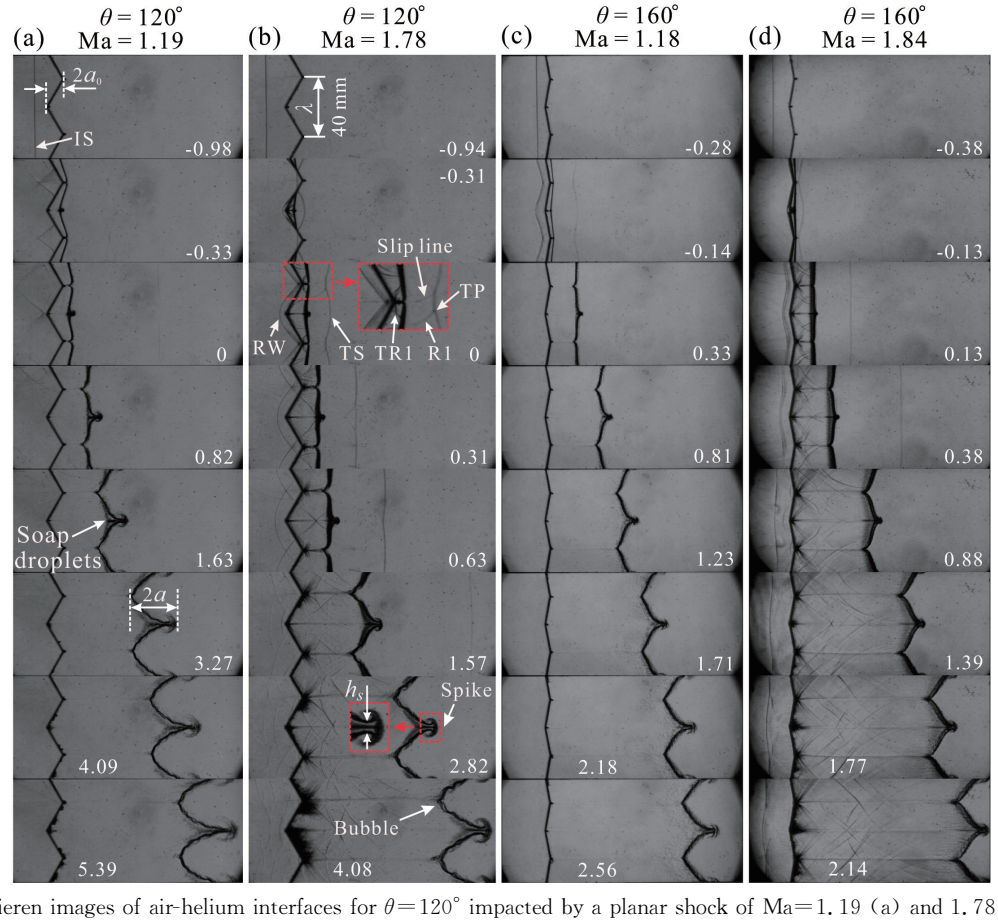

Fig. 2 Schlieren images of air-helium interfaces for $\theta=120°$ impacted by a planar shock of Ma=1.19 (a) and 1.78 (b), and for $\theta=160°$ impacted by a planar shock of Ma=1.18 (c) and 1.84 (d). IS, incident shock; TS, transmitted shock; R1, transverse shock waves generated by the interaction of TSs at the right vertex of the interface; TR1, transverse shock waves of R1 refracting through the interface; RW, reflected waves; a_0, initial interface amplitude; a, evolving interface amplitude; λ, interface wavelength; h_s, spike stem width. The numbers denote the dimensionless time.

2.1 Interface morphology and features

The evolution of the shocked interface with time is displayed in Fig. 2. Note that only four schlieren sequences ($\theta=120°$ with Ma=1.19 and 1.78, and $\theta=160°$ with Ma = 1.18 and 1.84) are shown here, because for the same initial amplitude, the qualitative

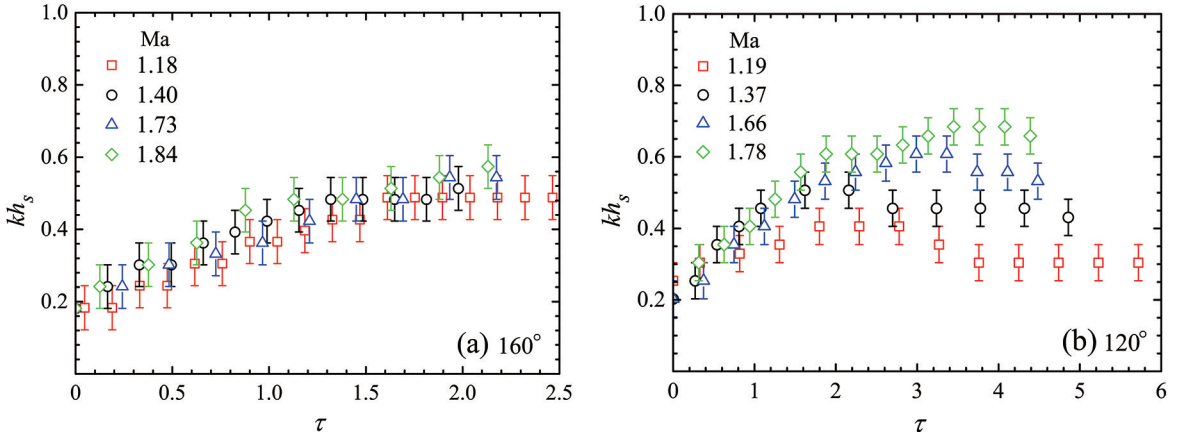

Fig. 3　Time variation of the spike stem width h_s at different Mach numbers for the small (a) and large (b) amplitude in dimensionless form

developments of the interface for cases of Ma ~ 1.4 and 1.7 are similar to those for cases of Ma ~ 1.2 and 1.8, respectively, and are omitted here. Taking the case of $\theta=120°$ and Ma = 1.78 as an example to discuss the evolution process, when the incident shock wave (IS) propagates along the air-helium interface, the transmitted shock wave (TS) moving downstream and the reflected waves (RW) moving upstream are generated. The TSs interact with each other at the right vertex of the interface, resulting in the formation of two new shocks (R1 is the transverse shock wave) connected by a Mach stem and two triple points (TP) (Fig. 2(b) at $\tau=0$, $\tau=kV_0^E(t-t^*)$ with k ($=2\pi/\lambda$) the wavenumber, t^* the time when the phase reversal is just completed, and V_0^E the experimental linear growth rate which will be discussed later). The slip line connecting the triple point is observed, which is the specific feature under the conditions of the high amplitude and moderate Mach numbers ($\theta=120°$ and Ma = 1.66, 1.78). The slip line is not observed for other cases, even for the small amplitude at Ma = 1.84. The shock R1 passes through the interface and generates another transverse shock wave (TR1). When the IS passes across the interface, phase reversal a specific phenomenon in the heavy-light configuration starts. The spike (a heavy fluid penetrating a light one) occurs in the middle and grows quickly in the direction of the post-shock flow, whereas the bubble (a light fluid penetrating a heavy one) develops in the opposite direction to the spike. As time proceeds, lots of small vortices appear on the inclined interface. Because more baroclinic vorticity is deposited on the interface with high initial amplitude, the vortex pair at the spike tip is more obvious.

From the comparison of the schlieren sequences shown in Fig. 2(c) and (d), the shock Mach number has a limited effect on the interface morphology for the small initial amplitude. However, for the high initial amplitude, as the shock Mach number increases, the vortex pair at the spike tip is more obvious, and the spike stem width (h_s, as defined as the distance of the spike stem, as shown in Fig. 2(b) at $\tau=2.82$) is wider. The spike stem width can reflect the size of the vortex to some extent. The time variation of the h_s in dimensionless form for cases of small and high initial amplitudes is shown in Fig. 3, in which the h_s is scaled as kh_s. For the small amplitude, the h_s first increases and then seems to be saturated within the time studied, and the shock Mach number has limited effect on the growth of the h_s. For the high initial amplitude, the h_s first experiences two stages similar to the case of the small amplitude, but it then decreases and finally is saturated. The rapid increase of the h_s at early times is due to the formation of the spike from the sharp corner on the left side of the interface. In this process, the spike stem grows from scratch and experiences rapid growth until it is saturated. Then, the spike continues to develop, and the stem is elongated in the streamwise direction with the reduction of the stem width due to the mass conservation. Finally the stem width enters an approximate saturation stage. Note that the h_s increases as the shock Mach number increases, because more vorticity is generated, and more fluids at the spike stem are entrained into the vortex pair.

So far, we have not found a connection between the spike stem width growth and amplitude growth.

Tab. 2 Linear growth rates obtained from experiments and theories for eight cases. V_0^E, V_0^{MB}, V_0^R, V_0^H and V_0^{New} are growth rates obtained from the experiments, the MB model, the Rikanati model, the Holmes model and the new model, respectively. F^R, F^H and F^N are the reduction factors of the Rikanati model, the Holmes model and the new model, respectively. The unit of the velocity is m/s.

θ	Ma	V_0^E	V_0^{MB}	V_0^R	V_0^H	V_0^{New}}	F^R	F^H	F^N
160	1.18	22.6±1.8	21.3	—	—	—	—	—	—
	1.40	39.4±1.5	39.3	—	—	—	—	—	—
	1.73	57.7±2.6	58.5	—	—	—	—	—	—
	1.84	59.9±1.5	63.4	—	—	—	—	—	—
120	1.19	52.0±1.8	63.8	51.3	58.8	47.3	0.80	0.92	0.74
	1.37	85.9±2.6	113.6	94.7	98.9	82.5	0.83	0.87	0.73
	1.66	119.0±2.1	166.9	142.5	136.8	116.8	0.85	0.82	0.70
	1.78	124.8±2.8	178.1	152.6	142.6	122.2	0.86	0.80	0.69

2.2 Linear growth of the amplitude

After the phase reversal, the amplitude grows with time and a linear growth is usually observed. For the light-heavy configuration in which the phase reversal is absent, Richtmyer[1] proposed the impulsive model to predict the linear growth rate, which can be expressed as

$$V_0^I = kA^+ U_c a_0^+ \tag{1}$$

where the post-shock amplitude $a_0^+ = a_0(1-U_c/U_i)$ with U_c and U_i being the jump velocity of the interface and the incident shock velocity, respectively, and A^+ is the post-shock Atwood number. Meyer & Blewett[37] found that the impulsive model is not applicable to the heavy-light case, unless a_0^+ is replaced by $(a_0+a_0^+)/2$, and they proposed the MB model, which is described as

$$V_0^{MB} = k\,|A^+|\,U_c\,\frac{a_0+a_0^+}{2} \tag{2}$$

The linear growth rates obtained from the linear fitting of the experimental data and from the MB model are listed in Tab. 2. For the small initial amplitude, because a chevron interface has a dominant mode[28,31], the MB model gives good predictions for all Mach numbers, that is, the Mach number has very limited effects on the linear growth rate. However, for the high initial amplitude, the MB model overestimates the linear growth for all cases even for the Mach number of 1.19. The high amplitude effect[43] and the secondary compressibility effect[43,49] are believed to have caused the discrepancy.

To evaluate the high amplitude effect, based on a vorticity deposition model, Rikanati et al[43] proposed a model (the Rikanati model) applicable for both sinusoidal and sawtooth interfaces with various amplitudes, which can be described as

$$V_0^R = V_0^{MB} \times F^R \tag{3}$$

where F^R is a reduction factor, defined as the ratio of the initial tip velocity to the tip velocity obtained by the incompressible linear model[28,43]. The predictions from the Rikanati model for the high initial amplitude are listed in tab., from which one can observe that the Rikanati model can only predict the linear growth of the high initial amplitude when the shock Mach number is low. As the shock Mach number increases, the Rikanati model overestimates the linear growth rate, which means the secondary compressibility effect also reduces the growth rate and cannot be neglected at moderate Mach numbers. By considering the relationship between velocities of shocks and interfaces, Holmes et al[49] constructed an empirical model (the Holmes model) for heavy-light cases, which can be expressed as

$$V_0^H = V_0^{MB} \times F^H \tag{4}$$

where $F^H = 1/[1+V_0^{MB}/(U_t-U_c)]$ with U_t being the transmitted shock velocity. From values in table 2, it is found that the Holmes model always overestimates experimental values, especially for stronger shock waves. As a result, for the high initial amplitude at moderate or high Mach numbers, both the high amplitude effect and the secondary compressibility effect must be considered. We combine two reduction factors (F^R and F^H) together, and propose a new model,

$$V_0^{New} = V_0^{MB} \times F^R \times F^H = V_0^{MB} \times F^N \tag{5}$$

As shown in Tab. 2, the new model gives a good prediction to the linear growth rate when Ma$\geqslant$1.37, but it slightly underestimates the linear growth rate for

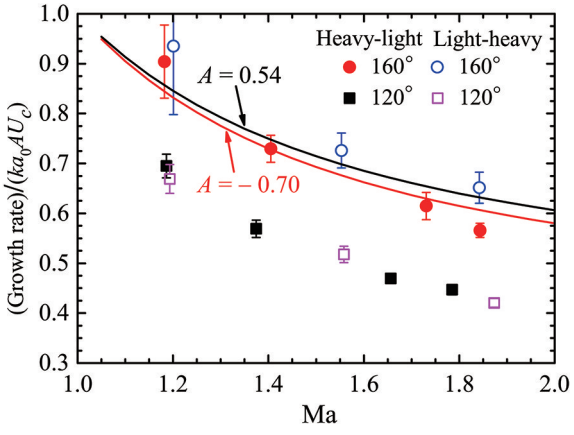

Fig. 4 Comparison of the experimental linear growth rates scaled by the value predicted from the uncompressed impulsive model between the heavy-light case and the light-heavy case[45]. The theoretical curves for the small amplitude are obtained based on the typical experimental condition for the heavy-light (light-heavy) case at the pre-shock Atwood number of −0.70 (0.54).

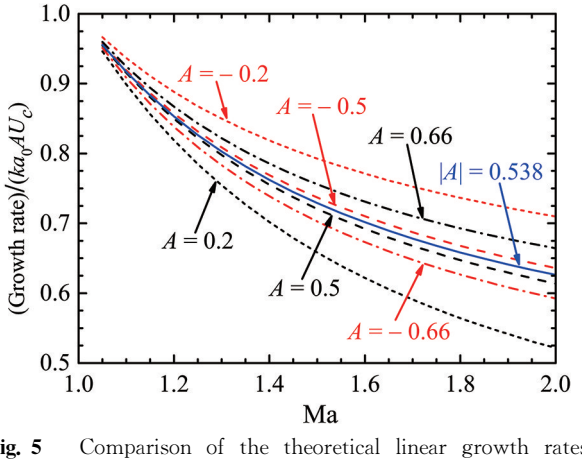

Fig. 5 Comparison of the theoretical linear growth rates predicted by the impulsive model for the air-SF_6 interface and the MB model for the air-helium interface scaled by the values predicted from the uncompressed impulsive model at different Atwood numbers and Mach numbers.

Ma=1.19 with a relative error of 9.1%.

From the discussion above, when the high initial amplitude is imposed on the interface, the high amplitude effect will cause the deviation of the experimental value from the prediction by the MB model. Moreover, under the conditions of high initial amplitudes and high shock Mach numbers, the transverse shock waves are prominent, and they propagate along the interface, bringing about the secondary compressibility effect which also inhibits the growth rate[26,44,49,50]. With the increase of the Mach number, the shock proximity effect[43,46] may occur and inhibit the growth of spikes (heavy-light case) or bubbles (light-heavy case). Rikanati et al[43] and Glendinning et al[46] proposed a parameter $\epsilon = V_0^{MB}/(U_t - U_c)$ to estimate the shock proximity effect. When ϵ is close to zero, the shock proximity effect is negligible, but when ϵ is close to or exceeds unity, the shock proximity effect needs to be considered. In our present work, the largest ϵ occurs in the case of $\theta = 120°$ and Ma=1.78, and ϵ is 0.25, which is much less than unity. Thus, the shock proximity effect is insignificant for heavy-light interfaces, which is different from light-heavy cases.

2.3 Compressibility effect on the amplitude growth

It is known that the compressibility effect caused by the incident shock wave will reduce the linear growth rate compared with the uncompressed case. The compressibility effect induced by the incident shock on the reduction of the linear growth rate of air-helium interfaces can be highlighted in Fig. 4, in which the growth rate is scaled by the result predicted from the uncompressed impulsive model (ka_0AU_c). As the Mach number increases, the experimental linear growth rates deviate more from the uncompressed impulsive model, because the increase of the Mach number will result in stronger compressibility. For small initial amplitudes, the compressibility effect on the reduction of the linear growth rates can be reflected by the ratio of the value predicted by the MB model and the value predicted by the uncompressed impulsive model, and this ratio (ξ) is $(A^+/A)[1-\frac{1}{2}(U_c/U_i)]$[49]. There are two sources about the compressibility. The first factor A^+/A is due to the material compression, and the second factor is due to the geometric compression of the perturbations at the interface by the shock and is represented by the average of the pre- and post-shock amplitudes[49]. Furthermore, the corresponding results of the light-heavy case (air-SF_6 interface experi-ments)[45]. The discrepancy between the experimental value and the prediction from the uncompressed impulsive model is magnified as the shock Mach number increases. For the light-heavy interface with small initial amplitudes, the compressibility effect on the reduction of the linear growth rates can be reflected by the ratio of the value predicted by the impulsive model to the value predicted by the uncompressed impulsive model, and this ratio (ξ) is $(A^+/A)(1-U_c/U_i)$. Different from the heavy-light case, the geometric compression of the perturbations in the

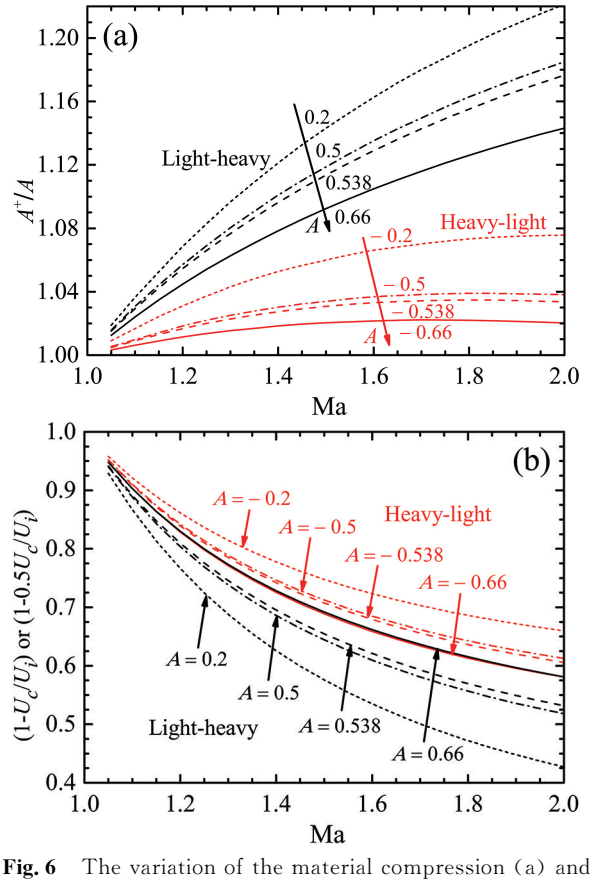

Fig. 6 The variation of the material compression (a) and geometric compression of the interface (b) with the Atwood number for both the heavy-light and light-heavy cases

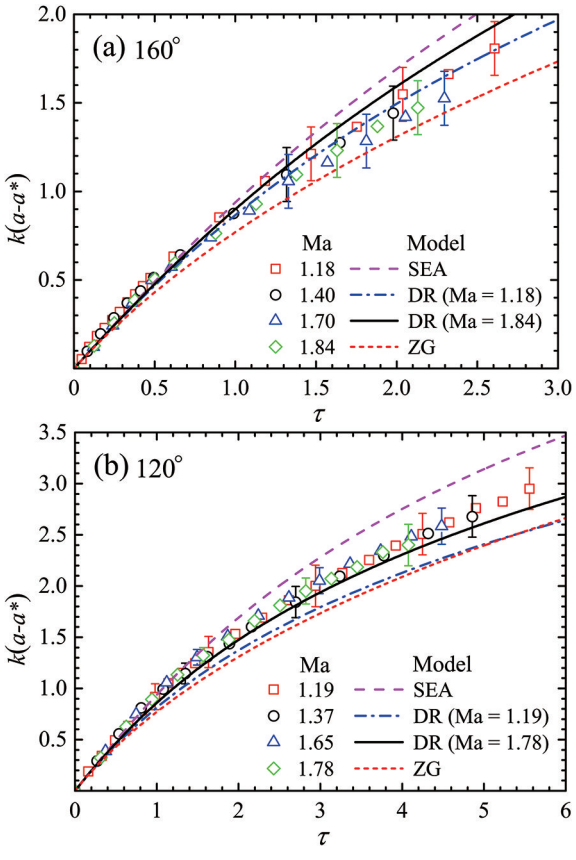

Fig. 7 Comparison of the experimental amplitude growths and theoretical predictions in the linear and nonlinear stage for the small (a) and large (b) amplitude

light-heavy case is presented only by the post-shock amplitude. For high initial amplitudes, the experimental linear growth rates deviate more heavily from the predictions by the uncompressed model, because except for the compressibility effect induced by the incident shock, the high amplitude effect and the secondary compressibility effect caused by transverse waves also reduce the linear growth rate.

The variation of the ratio ξ for the light-heavy and the heavy-light cases with the shock Mach number can be theoretically obtained for any given pre-shock Atwood number A. For air-helium interfaces in this work and air-SF_6 interfaces in the previous work[45], the pre-shock Atwood numbers are about -0.7 and 0.54, respectively, and the variations of the ratio ξ with the shock Mach number are plotted in Fig. 4. The theoretical curves coincide well with the experimental results. To better compare the compressibility effect caused by the incident shock wave under the light-heavy and heavy-light cases, for small initial amplitudes, the variation of the ratio ξ at different Atwood numbers as a function of the Mach number is plotted in Fig. 5. It is found that the reduction of the growth rate caused by the compressibility effect for the light-heavy and heavy-light cases is different. As $|A|$ increases, the ratio ξ increases for the light-heavy case, whereas it reduces for the heavy-light case. Specifically, when the $|A|$ is 0.538, the growth rate reductions for these two cases are nearly the same.

Besides, the variation of the material compression factor (A^+/A) and the geometric compression factor $[1-U_c/U_i$ or $1-\frac{1}{2}(U_c/U_i)]$ with the Atwood number is presented in Fig. 6(a) and (b), respectively. For both light-heavy and heavy-light cases, the A^+/A is larger than unity, that is, the material compression increases the growth rate. However, the geometric compression factor is smaller than unity, and the contribution of the geometric compression to the reduction of the growth rate exceeds the contribution of the material compression to the increase of the growth rate. As a result, the compressibility effect always reduces the

linear growth rate. Note that the material compression factor decrease with the increase of the $|A|$ for both light-heavy and heavy-light cases. However, as the $|A|$ increases, the geometric compression factor decrease for the heavy-light case, whereas it increases for the light-heavy case. Because the geometric compression dominates the compressibility effect on the linear growth rate, the ratio ξ decrease in the light-heavy case as the Atwood number increases, whereas it increases in the heavy-light case, as shown in Fig. 5.

2.4 Nonlinear growth of the amplitude

After the linear growth stage, the interface amplitude enters a nonlinear regime. To predict the amplitude nonlinear behavior, Sadot et al[24] proposed a nonlinear model (the SEA model) based on experiments and potential theories[23,51],

$$V_{b/s}^{\mathrm{SEA}}(t)=V_0\frac{1+\tau}{1+(1\pm|A^+|)\tau+F_{b/s}^{\mathrm{SEA}}\tau^2} \tag{6}$$

where

$$F_{b/s}^{\mathrm{SEA}}(t)=\frac{1\pm|A^+|}{(2\pi C)(1+|A^+|)}$$

with $C=1/(3\pi)$ for $A^+\gtrsim 0.5$, $1/(2\pi)$ for $A^+\to 0$. The subscript 'b' and 's' are for bubbles and spikes, respectively.

Dimonte & Ramaprabhu[52] proposed a nonlinear model (the DR model) according to numerical simulations. The model is expected to be applicable to cases of various ka_0^+ and A^+, and can be expressed as

$$V_{b/s}^{\mathrm{DR}}(t)=V_0\frac{1+(1\mp|A^+|)\tau}{1+C_{b/s}\tau+(1\mp|A^+|)F_{b/s}\tau^2} \tag{7}$$

where

$$C_{b/s}=\frac{4.5\pm|A^+|+(2\mp|A^+|)\,|ka_0^+|}{4},$$

$$F_{b/s}=1\pm|A^+|.$$

By considering the governing equations for incompressible, inviscid and irrotational fluids with arbitrary density ratio in two dimensions[53], Zhang & Guo[54] studied the asymptotic large-time behavior of the shocked interface, and described the growth rates of spikes and bubbles by a universal model (the ZG model),

$$V_{b/s}^{\mathrm{ZG}}(t)=V_0\frac{1}{1+\alpha\tau} \tag{8}$$

where

$$\alpha=\left[\frac{3}{4}\frac{(1+|A^+|)(3+|A^+|)}{[3+|A^+|+\sqrt{2}(1+|A^+|)^{1/2}]}\right]\times$$

$$\left[\frac{[4(3+|A^+|)+\sqrt{2}(9+|A^+|)(1+|A^+|)^{1/2}]}{[(3+|A^+|)^2+2\sqrt{2}(3-|A^+|)(1+|A^+|)^{1/2}]}\right] \tag{9}$$

Fig. 7 shows the time variation of the amplitude growth at early and late times in dimensionless form. The amplitude is scaled as $k(a-a^*)$ with a^* being the amplitude at t^*. Note that the amplitude growth in Fig. 7 starts when the phase reversal ends. The experimental data for both small and large amplitudes collapse well, showing that the Mach number has little effect on the amplitude nonlinear growths, because the transmitted and reflected waves have moved far away from the interface in the nonlinear phase. Note that the SEA model and the ZG model are only related to A^+, and A^+ for different cases are similar in this work Therefore, only one theoretical curve is shown to avoid confusion. However, the DR model relates not only to A^+, but also to ka_0^+, and thus, it will give different predictions for different ka_0^+. In this work, the predictions obtained from the DR model for cases of Ma $\sim$ 1.2 and $\sim$ 1.8 are given, while the theoretical curves from the DR model for other shock Mach numbers are located between the cases of Ma $\sim$ 1.2 and $\sim$ 1.8, and are omitted. It can be found that for both two initial amplitudes, the SEA model gives good predictions to the early growth behavior until $\tau\approx 1.5$, but then overestimates the nonlinear growth. The ZG model underestimates the growth nearly from the start.

The prediction by the DR model increases as the shock Mach number increases. For small initial amplitudes, the DR model can give a better prediction only for low Mach number conditions, whereas for high initial amplitudes, it predicts the growth of the perturbation better for high Mach number conditions. As a result, these nonlinear models mentioned above are not available to predict the perturbation growth for the current chevron interface, especially at late stages, because the chevron interface has infinite many modes initially. At early stages, since the chevron interface has a dominant mode and each mode develops independently, the nonlinear model can give a good prediction to the linear growth rate. When the perturbation growth enters the nonlinear regime, the high-order modes will interact with each other, and the mode coupling and competition greatly complicate the flow, resulting in the failure of nonlinear models. Therefore, it is quite necessary

to develop nonlinear models by considering the mode coupling and competition for a multi-mode interface.

3 Conclusion

Shock tube experiments of a periodic air/helium chevron interface impacted by a planar shock wave are conducted to highlight effects of the initial amplitude and the compressibility on the perturbation growth. Two initial amplitudes and four different incident shock Mach numbers ranging from 1.2 to 1.9 are involved. The periodic chevron interface is created using the soap film technique, and the post-shock flows are captured by a high-speed schlieren system.

After the incident shock wave passes across the air-helium interface, the phase reversal which is the specific feature in the heavy-light interface is observed. The shock Mach number has limited effect on the interface morphology and feature when initial amplitudes are small. For high initial amplitudes, the transverse waves are prominent, which will introduce secondary compressibility effect. Under the high initial amplitude and strong shock wave conditions, the slip lines connecting the triple points are observed, and the vortex pair at the spike tip are more obvious because more baroclinic vorticity is deposited on the interface. The variation of the spike stem width for different cases is compared. The results show that the spike stem width is almost not affected by the Mach number in the small amplitude cases. For high initial amplitudes, the increase of the shock Mach number causes a larger spike stem width, because a strong shock wave will induce more vorticity at the spike tip and more fluids at the spike stem are entrained into the vortex pair.

The linear growth rate of the perturbation is measured and compared with the prediction from the linear model. For small initial amplitudes, the Mach number has limited effect on the reliability of the linear model. For high initial amplitudes, however, the linear model is generally invalid because the high amplitude effect and the secondary compressibility effect induced by transverse waves will additionally reduce the linear growth rate. By considering the high amplitude effect and the high Mach number effect, the linear growth rate of the interface with high initial amplitude impacted by a strong shock wave can be well predicted. The compressibility effect induced by the incident shock wave can be illustrated by the material compression and the geometric compression of the interface. For both light-heavy or heavy-light interfaces, the material compression increases the linear growth rate, and as the absolute value of the Atwood number increases, the effect of material compression is weakened. The geometric compression of the interface reduces the linear growth rate. For light-heavy interfaces, the effect of geometric compression on growth reduction is weakened as the Atwood number increases. However, for heavy-light interfaces, the effect of geometric compression on the growth reduction is strengthened as the absolute value of the Atwood number increases. Since geometric compression plays a more significant role than material compression in changing the linear growth rate, the compressibility effect induced by incident shock wave always reduces the linear growth rate. In the nonlinear regime, some nonlinear models originally proposed for predicting the growth of the single-mode interface are tested, and the validity of the models are verified to be valid only at very early stages, because the initial interface in this work is multi-mode and the developments of high-order modes cannot be ignored at late stages.

Acknowledgements

This work was supported by the National Natural Science Foundation of China (Nos. 11772329, 11625211).

References

[1] Richtmyer R D. Taylor instability in shock acceleration of compressible fluids. Commun. Pure Appl. Math., 1960, 13: 297-319.

[2] Meshkov E E. Instability of the interface of two gases accelerated by a shock wave. Fluid Dyn., 1969, 4: 101-104.

[3] Arnett D. The role of mixing in astrophysic. Annu. Rev. Astron., Astrophys, 2000, 127: 213-217.

[4] Shimoda J, Inoue T, Ohira Y, et al. On cosmicray production efficiency at supernova remnant shocks propagating into realistic diffuse interstellar medium. Astrophys. J., 2015, 803: 98-103.

[5] Khokhlov A M, Oran E S, Thomas G O. Numerical simulation of deflag ration to detonation transition: The role of shock-flame interactions in turbulent flames. Combust. Flame, 1999, 117: 323-339.

[6] Yang J, Kubota T, Zukoski E E. Application of shock

induced mixing to supersonic combustion. AIAA J., 1993, 31: 854-862.

[7] Curran E T, Heiser W H, Pratt D T. Fluid phenomena in scram jet combustion systems. Annu. Rev. Fluid Mech., 1996, 28: 323-360.

[8] Oakley B, Brooks J, Anderson P, et al. Shock tube investigation of hydrodynamic issues related to inertial confinement fusion. Shock Waves, 2000, 10: 377-387.

[9] Lindl J, Landen O, Edwards J, et al. Review of the national ignition campaign 2009-2012. Phys. Plasmas, 2014, 21: 020501.

[10] Zabusky N J. Vortex paradigm for accelerated in homogeneous flows: Visio metrics for the Rayleigh-Taylor and Richtmyer-Meshkov environments. Annu. Rev. Fluid Mech., 1999, 31: 495-536.

[11] Brouillette M. The Richtmyer-Meshkov instability. Annu. Rev. Fluid Mech., 2002, 34: 445-468.

[12] Ranjan D, Oakley J, Bonazza R. Shock-bubble interactions. Annu. Rev. Fluid Mech., 2011, 43: 117-140.

[13] Zhou Y. Rayleigh-Taylor and Richtmyer-Meshkov instability induced flow, turbulence, and mixing. Ⅰ. Phys. Rep., 2017.

[14] Zhou Y. Rayleigh-Taylor and Richtmyer-Meshkov instability induced flow, turbulence, and mixing. Ⅱ. Phys. Rep., 2017.

[15] Zhai Z, Zou L, Wu Q, et al. Review of experimental Richtmyer-Meshkov instability in shock tube: From simple to complex. P. I. Mech. Eng. C-J. Mec., 2018, 232: 2830-2849.

[16] Brouillette M, Sturtevant B. Experiments on the Richtmyer-Meshkov instability: Small-scale perturbations on a plane interface. Phys. Fluids A, 1993, 5: 916-930.

[17] Vanderboomgaerde M, Souffland D, Mariani C, et al. Investigation of the Richtmyer-Meshkov instability with stereolithographed interfaces. Phys. Fluids, 2014, 26: 024109.

[18] Ranjan D, Anderson M, Oakley J, et al. Experimental investigation of a strongly shocked gas bubble. Phys. Rev. Lett., 2005, 94: 184507.

[19] Zhai Z, Wang M, Si T, et al. On the interaction of a planar shock with a light polygonal interface. J. Fluid Mech., 2014, 757: 800-816.

[20] Collins B D, Jacobs J W. PLIF flow visualization and measurements of the Richtmyer-Meshkov instability of an air/SF6 interface. J. Fluid Mech., 2002, 464: 113-136.

[21] Balakumar B J, Orlicz G C, Tomkins C D, et al. Dependence of growth patterns and mixing width on initial conditions in Richtmyercmeshkov unstable fluid layers. Physica Scripta T132, 2008: 014013.

[22] McFarland J, Reilly D, Creel S, et al. Experimental investigation of the inclined interface Richtmyer-Meshkov instability before and after reshock. Exp. Fluids, 2014, 55: 1640-1653.

[23] Jacobs J W, Sheeley J M. Experimental study of in compressible Richtmyer-Meshkov instability. Phys. Fluids, 1996, 8: 405-415.

[24] Sadot O, Erez L, Alon U, et al. Study of nonlinear evolution of single-mode and two-bubble interaction under Richtmyer-Meshkov instability. Phys. Rev. Lett., 1998, 80: 1654-1657.

[25] Jacobs J W, Krivets V V. Experiments on the late time development of single-mode Richtmyer-Meshkov instability. Phys. Fluids, 2005, 17: 034105.

[26] Motl B, Oakley J, Ranjan D, et al. Experimental validation of a Richtmyer-Meshkov scaling law over large density ratio and shock strength ranges. Phys. Fluids, 2009, 21: 126102.

[27] Liu L, Liang Y, Ding J, et al. An elaborate experiment on the single-mode Richtmyer-Meshkov instability. J. Fluid Mech., 2018, 853: R2.

[28] Luo X, Dong P, Si T, et al. The Richtmyer-Meshkov instability of a 'V' shaped air/SF_6 interface. J. Fluid Mech., 2016, 802: 186-202.

[29] Guo X, Ding J, Luo X, et al. Evolution of a shocked multimode interface with sharp corners. Phys. Rev. Fluids 3, 2018: 114004.

[30] Luo X, Liang Y, Si T, et al. Effects of non-periodic portions of interface on Richtmyer-Meshkov instability. J. Fluid Mech., 2019, 861: 309-327.

[31] Liang Y, Zhai Z, Ding J, et al. Richtmyer-Meshkov instability on a quasi-single-mode interface. J. Fluid Mech., 2019, 872: 729-751.

[32] McFarland J A, Reilly D, Black W, et al. Modal interactions between a large-wavelength inclined interface and small-wavelength multimode perturbations in a Richtmyer-Meshkov instability. Phys. Rev. E, 2015, 92: 013023.

[33] Reilly D, McFarland J, Mohaghar M, et al. The effects of initial conditions and circulation deposition on the inclined-interface reshocked Richtmyer-Meshkov instability. Exp. Fluids, 2015, 56: 168.

[34] Mohaghar M, Carter J, Musci B, et al. Evaluation of turbulent mixing transition in a shock-driven variable-density flow. J. Fluid Mech., 2017, 831: 779-825.

[35] Mohaghar M, Carter J, Pathikonda G, et al. The transition to turbulence in shock-driven mixing: effects of Mach number and initial conditions. J. Fluid Mech., 2019, 871: 595-635.

[36] Guo X, Zhai Z, Si T, et al. Bubble merger in initial Richtmyer-Meshkov instability on inverse-chevron interface. Phys. Rev. Fluids, 2019, 4: 092001(R).

[37] Meyer K A, Blewett P J. Numerical investigation of the

stability of a shock-accelerated interface between two fluids. Phys. Fluids, 1972, 15: 753-759.
[38] Jourdan G, Houas L. High-amplitude single-mode perturbation evolution at the Richtmyer-Meshkov instability. Phys. Rev. Lett., 2005, 95: 204502.
[39] Mariani C, Vanderboomgaerde M, Jourdan G, et al. Investigation of the Richtmyer-Meshkov instability with stereolithographed interfaces. Phys. Rev. Lett., 2008, 100: 254503.
[40] Ma D, Ding J, Luo X. Study on Richtmyer-Meshkov instability at heavy/light single-mode interface. Sci. Sin. Phys. Mech. Astron., 2020, 50: 104705.
[41] Mikaelian K O. Richtmyer-Meshkov instability of arbitrary shapes. Phys. Fluids, 2005, 17: 034101.
[42] Aleshin A N, Lazareva E V, Zaitsev S G, et al. Linear, nonlinear, and transient stages in the development of the Richtmyer-Meshkov instability. Sov. Phys. Dokl., 1990, 35: 159-161.
[43] Rikanati A, Oron D, Sadot O, et al. High initial amplitude and high Mach number effects on the evolution of the single-mode Richtmyer-Meshkov instability. Phys. Rev. E, 2003, 67: 026307.
[44] Sadot O, Rikanati A, Oron D, et al. An experimental study of the high Mach number and high initial amplitude effects on the evolution of the single-mode Richtmyer-Meshkov instability. Laser Part. Beams, 2003, 21: 341-346.
[45] Guo X, Zhai Z, Ding J, et al. Effects of transverse shock waves on early evolution of multi-mode chevron interface. Phys. Fluids, Submitted.
[46] Glendinning S G, Bolstad J, Braun D G, et al. Effect of shock proximity on Richtmyer-Meshkov growth. Phys. Plasmas, 2003, 10: 1931-1936.
[47] Zhai Z, Dong P, Si T, et al. The Richtmyer-Meshkov instability of a 'V' shaped air/helium interface subjected to a weak shock. Phys. Fluids, 2016, 28: 082104.
[48] Isenberg C. The Science of Soap Films and Soap bubbles. New York: Dover publications, INC., 1992.
[49] Holmes R L, Dimonte G, Fryxell B, et al. Richtmyer-Meshkov instability growth: Experiment, simulation and theory. J. Fluid Mech., 1999, 389: 55-79.
[50] Stanic M, Stellingwerf R F, Cassibry J T, et al. Scale coupling in Richtmyer-Meshkov flows induced by strong shocks. Phys. Plasmas, 2012, 19: 082706.
[51] Alon U, Hecht J, Mukamel D, et al. Scale invariant mixing rates of hydrodynamically unstable interface. Phys. Rev. Lett., 1994, 72: 2867-2870.
[52] Dimonte G, Ramaprabhu P. Simulations and model of the nonlinear Richtmyer-Meshkov instability. Phys. Fluids, 2010, 22: 014104.
[53] Layzer D. On the instability of superposed fluids in a gravitational field. Astrophys. J., 1955, 122: 1-12.
[54] Zhang Q, Guo W. Universality of finger growth in two dimensional Rayleigh-Taylor and Richtmyer-Meshkov instabilities with all density ratios. J. Fluid Mech., 2016, 786: 47-61.

可压缩性对激波冲击 V 形空气/氦气界面演化的影响

郭 旭,翟志刚,罗喜胜
中国科学技术大学近代力学系,安徽合肥 230027

摘要:通过实验在激波管中研究了平面激波冲击下 V 形空气/氦气界面的演化过程,重点关注了可压缩性和初始振幅对扰动增长的影响.结果表明:对于小振幅情况,马赫数基本不影响线性模型的有效性;但对于大振幅情况,由于大振幅效应降低了线性增长率,这使得线性模型在低马赫数时就失效,而且随着马赫数的提高,线性模型与实验增长率之间的差异会越来越大.在考虑大振幅效应和高马赫数效应后,强激波冲击下大振幅界面的扰动增长率可以被很好地预测.入射激波引起的可压缩性可以通过物质压缩和几何压缩两项来反映,且几何压缩被证实起主导作用.针对单模界面的一些非线性模型被用来预测 V 形界面的振幅增长,但它们只在初期是有效的,到中后期就偏离了实验结果.

关键词:Richtmyer-Meshkov 不稳定性;多模

GUO Xu: PhD candidate. Research field: Experimental fluid mechanics. E-mail: clguoxu@mail.ustc.edu.cn
ZHAI Zhigang: Corresponding author, PhD/professor. Research field: Experimental fluid mechanics. E-mail: sanjing@ustc.edu.cn
LUO Xisheng: PhD/professor. Research field: Aerodynamics, multiphase hydrodynamics. E-mail: xluo@ustc.edu.cn